The gigantic Rashba effect of surface states energetically buried in the topological insulator Bi_2Te_2Se

2014 New J. Phys. 16 065016

(http://iopscience.iop.org/1367-2630/16/6/065016)

New Journal of Physics
The open access journal at the forefront of physics
Deutsche Physikalische Gesellschaft DPG | IOP Institute of Physics

The gigantic Rashba effect of surface states energetically buried in the topological insulator Bi_2Te_2Se

K Miyamoto[1], T Okuda[1], M Nurmamat[2], M Nakatake[1], H Namatame[1], M Taniguchi[1,2], E V Chulkov[3,4,5], K A Kokh[6,7], O E Tereshchenko[7,8] and A Kimura[2]

[1] Hiroshima Synchrotron Radiation Center, Hiroshima University, 2-313 Kagamiyama, Higashi-Hiroshima 739-0046, Japan
[2] Graduate School of Science, Hiroshima University, 1-3-1 Kagamiyama, Higashi-Hiroshima 739-8526, Japan
[3] Departamento de Física de Materiales UPV/EHU, Centro de Física de Materiales CFM-MPC and Centro Mixto CSIC-UPV/EHU, 20080 San Sebastián/Donostia, Basque Country, Spain
[4] Donostia International Physics Center (DIPC), 20018 San Sebastián/Donostia, Basque Country, Spain
[5] Tomsk State University, 634050 Tomsk, Russia
[6] V.S. Sobolev Institute of Geology and Mineralogy, Siberian Branch, Russian Academy of Sciences, Koptyuga pr. 3, Novosibirsk, 630090, Russia
[7] Novosibirsk State University, ul. Pirogova 2, Novosibirsk, 630090, Russia
[8] Institute of Semiconductor Physics, Siberian Branch, Russian Academy of Sciences, pr. Akademika Lavrent'eva 13, Novosibirsk, 630090, Russia
E-mail: kmiyamoto@hiroshima-u.ac.jp, teresh@isp.nsc.ru and akiok@hiroshima-u.ac.jp

Received 28 January 2014, revised 20 March 2014
Accepted for publication 15 April 2014
Published 24 June 2014

New Journal of Physics **16** (2014) 065016
doi:10.1088/1367-2630/16/6/065016

Abstract

We have clarified that a topological insulator, Bi_2Te_2Se, shows two surface states with gigantic Rashba-type spin-splitting located at a binding energy deeper than the topological surface state. The magnitude of the Rashba parameter, as well as the momentum splitting, is found to be large enough to realize a number of nanometer-sized spintronic devices. This novel finding paves the way to studies of gigantic Rashba systems that are suitable for future spintronic applications.

Keywords: gigantic Rashba effect, spin-ARPES, topologial insulator

1. Introduction

Topological insulators and Rashba systems have attracted a great deal of attention as key materials to revolutionize spin current devices without external magnetic fields [1–4]. In these nonmagnetic materials, the spin degeneracy is lifted by spin-orbit interactions in combination with broken space inversion symmetry. These systems have been extensively studied in recent years by angle-resolved photoemission spectroscopy (ARPES), spin- and angle-resolved photoemission spectroscopy (spin-ARPES) and first-principles calculations [5–37]. In particular, the spin characteristics of the surface states have been discussed in detail. In ideal topological insulators and Rashba systems, the spins are completely oriented in-plane and normal to the electron momenta, forming a helical spin texture.

The ideal two-dimensional Rashba effect is explained by the Rashba Hamiltonian (H_R) [6].

$$H_R\left(\mathbf{k}\right) = \alpha_{\mathrm{R}}\sigma \cdot \left(\mathbf{k}_{\parallel} \times \mathbf{e}_z\right) \tag{1}$$

From the Hamiltonian, the Rashba effect leads to a spin-splitting of the parabolic band dispersion, as described below [6]

$$E_{\pm}\left(\mathbf{k}\right) = E_0 + \frac{\hbar^2\mathbf{k}^2}{2\,m^*} \pm \left|\alpha_{\mathrm{R}}\right|\left|\mathbf{k}\right| = E_0 + \frac{\hbar^2}{2\,m^*}\left(\left|\mathbf{k}\right| \pm k_0\right)^2 - E_{\mathrm{R}} \tag{2}$$

where, m^* and α_{R} are the effective mass and Rashba parameter. Here, k_0 and E_R are defined as $k_0 = \frac{m^*\left|\alpha_R\right|}{\hbar^2}$ and $E_R = \frac{m^*\alpha_{\mathrm{R}}^2}{2\hbar^2}$. In many cases, the Rashba parameter α_R is thought to be the most important for highly efficient spintronic devices such as spin-field-effect transistors (spin-FETs). Since the source–drain distance (L) of spin-FETs is required to be larger than the characteristic half-wavelength π/k_0 [2], and E_R is directly linked to the stability of the device operated at elevated temperatures, one should also pay more attention to k_0 and E_R. In fact, the spin-splitting size needs to be more than $k_0 = 0.1$ Å^{-1} and $E_R = 200$ meV in order to downsize the channel length to a few nanometers and to realize stable device operation at room temperature. However, the spin-splitting size is currently insufficient in the Rashba systems discovered so far, including the (111) surfaces of Au, Bi and Sb [6–13], as well as Bi/Ag(111)[14, 15] and bulk BiTeI, etc [16–20]. Therefore, as a first approach we need to discover Rashba systems with larger spin-splitting. In this context, topological insulators or similar compounds might have the potential to show a larger Rashba effect due to the much stronger spin-orbit interaction than in well-known Rashba systems.

Here, we present a deeper-lying surface state with gigantic Rashba spin-splitting in the topological insulator Bi_2Te_2Se, studied using state-of-the-art spin-ARPES. Previously, we clarified that the highly spin-polarized natures of topological surface states (TSSs) are persistent above and below the Dirac point in this material [23, 40]. These findings can be a platform for future studies on gigantic Rashba systems that are suitable for spintronic devices.

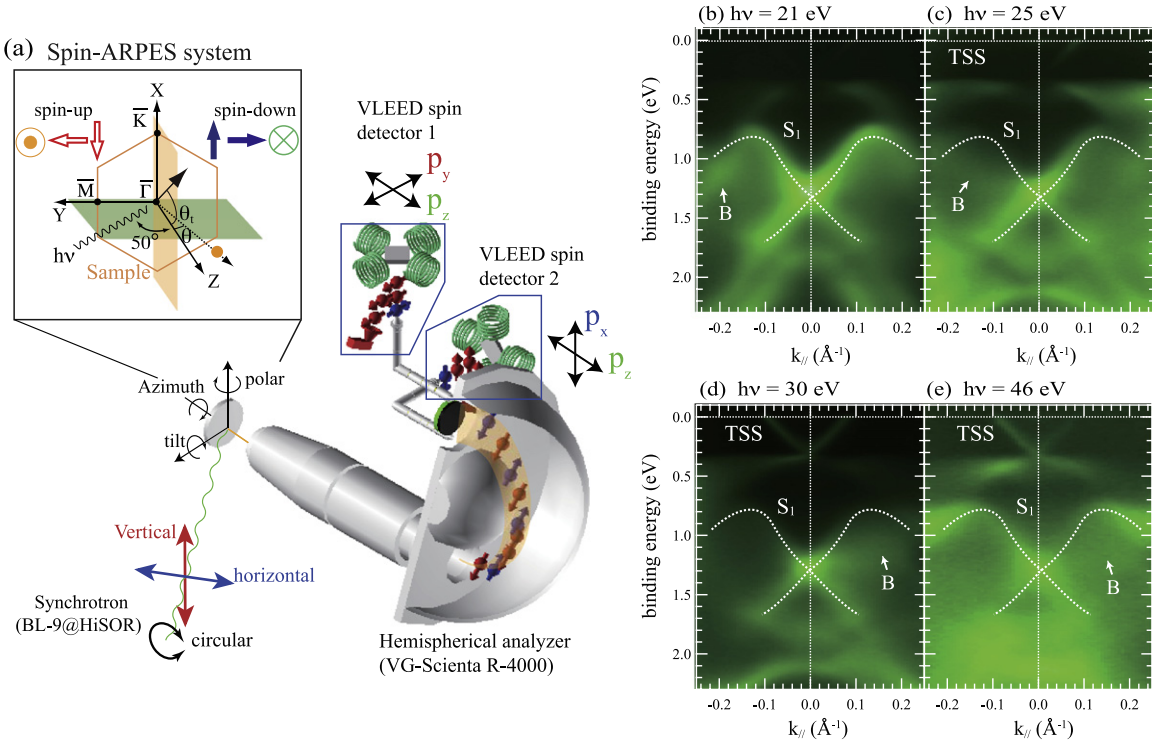

Figure 1. (a) Schematic of our efficient, spin-resolved spectroscopy machine, and the experimental geometry. (b)–(e) The energy-band dispersion curves along $\overline{\Gamma M}$ taken by a p-polarized synchrotron radiation light of $h\nu$ = 21, 25, 30 and 46 eV.

2. Experimental

The ARPES experiment was performed at the bending-magnet beam line (BL-7) with a hemispherical analyzer (VG Scienta SES 2002) at the Hiroshima Synchrotron Radiation Center (HSRC). The spin-ARPES experiment was done at the APPLE-II type variable polarization undulator beam line (BL-9B) at HSRC. Our spin-ARPES system is equipped with a hemispherical electron analyzer (VG Scienta R-4000) combined with a pair of very low energy electron diffraction (VLEED)-type spin detectors, and achieves much higher efficiency ($\epsilon \sim 10^{-2}$) than conventional Mott-type spin detectors ($\epsilon \sim 10^{-4}$) [41]. The spin-ARPES system can resolve both out-of-plane (P_z) and in-plane (P_x and P_y) spin polarization components with high angular and energy resolutions, as schematically shown in figure 1(a). The signs of the polar (θ) and tilt angles (θ_t) of the sample are defined as positive, in the case of anticlockwise rotation about the x axis and clockwise rotation about the y axis, respectively. The overall energy and angular resolutions for ARPES (ARPES and spin-ARPES) were set to 40 meV (20 meV) and 0.3° (0.75°) at BL-7 (BL-9B), and all measurements were performed at a sample temperature of 70 K. The samples were cleaved *in-situ* under an ultra-high vacuum below 1×10^{-8} Pa. ARPES at BL-7 was conducted using synchrotron radiation with photon energies ($h\nu$s) ranging from 21 to 60 eV. Spin-ARPES and ARPES at BL-9B were performed with a high-flux He-discharge lamp ($h\nu$ = 21.22 eV).

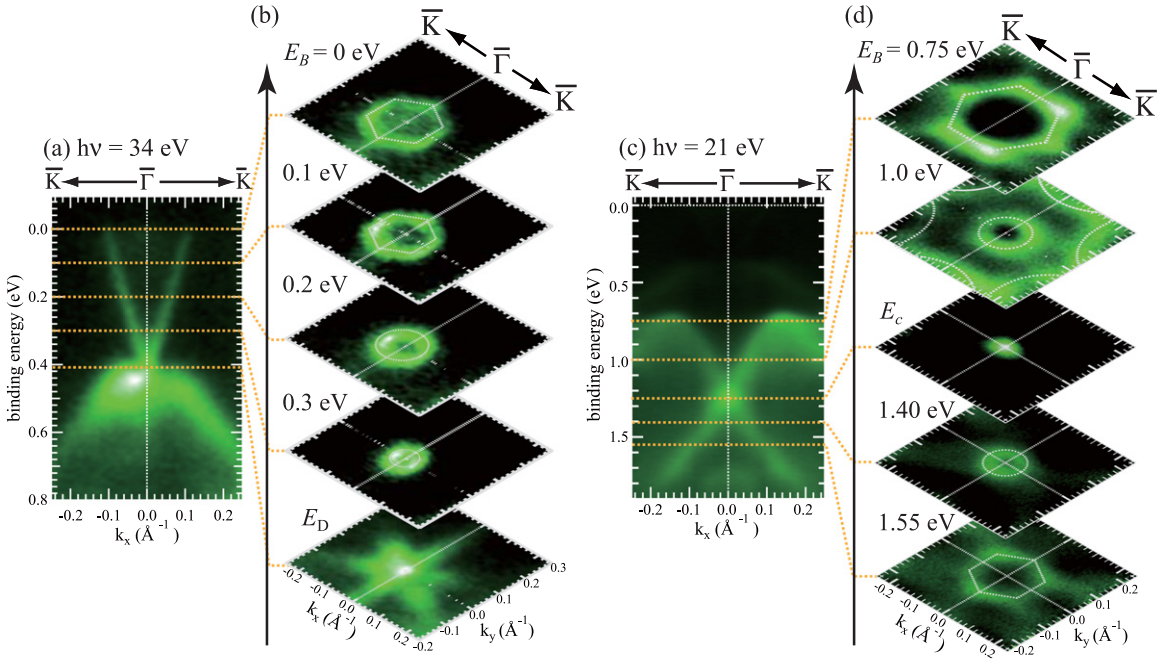

Figure 2. (a), (c) ARPES results taken by p-polarized light of two photon energies ($h\nu$ = 34, 21 eV) suitable for the observation of TSS and S_1 along $\overline{\Gamma K}$. (b), (d) The constant energy contours for two different surface states at several binding energies from 0 to 0.41 eV and from 0.75 to 1.55 eV.

3. Results and Discussion

Figures 1(b)–(e) show the selected ARPES results obtained by several photon energies along the $\overline{\Gamma M}$ line. The energy dispersion curve taken at 21 eV shows two upward-convex parabolic states (dashed line), as well as another upward-convex arc, with the energy maximum at a binding energy (E_B) of 1.75 eV, at the $\bar{\Gamma}$ point. In particular, two characteristic parabolic bands (S_1) with an energy maximum of E_B = 0.75 eV and a wavenumber of $\pm$0.135 Å are clearly observed, with a crossing at E_B = 1.25 eV at the $\bar{\Gamma}$ point. In figures 1(c)–(e), the results for $h\nu$ = 25, 35 and 46 eV present one TSS near the Fermi energy, as already reported by several groups [23, 24] and the parabolic band structure (S_1) without changing band shape. The weak broad, bulk band structure (B) is also observed close to the S_1 state below 1.25 eV. Note that the particular parabolic band S_1 can be observed with all photon energies in our study as keeping the energy maxima, the crossing point at the same energy, and the same k-position, which confirms its two-dimensional nature. More interestingly, the surface state S_1 is likely to show extremely large Rashba-type spin-splitting.

The two-dimensional slices in the **k** space for TSS and S_1 at several constant energies are shown in figure 2. Figure 2(b) demonstrates a typical hexagonal deformation of TSS, which evolves into a circular shape on approaching the crossing point. We find that the band dispersion along the $\overline{\Gamma K}$ line gradually becomes steeper toward E_F, while it is almost straight along the $\overline{\Gamma M}$ line, which actually reflects the deformation of constant energy contours (CECs). Near the crossing point, the bulk valence band forms a six-fold petal-like pattern. These results

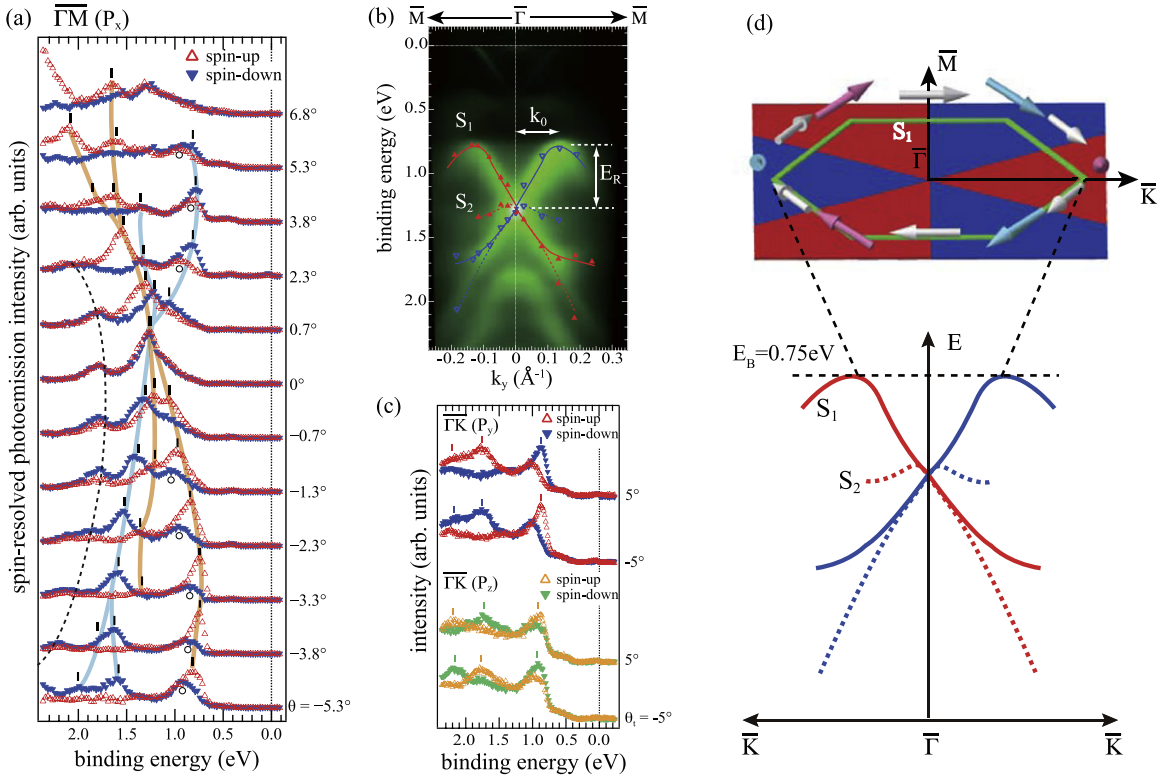

Figure 3. (a) Spin-resolved energy distribution curves (EDCs) of Bi_2Te_2Se along $\overline{\Gamma M}$ obtained by unpolarized He-Iα radiation. (b) The spin characters derived from the spin-resolved spectra in figure 3(a) are superimposed in E-k mapping by ARPES measurements with a He discharge lamp. (c) Spin-resolved EDCs along $\overline{\Gamma K}$ by unpolarized He-Iα radiation for spin components of P_y and P_z. The schematic diagrams of (d) show band dispersion along $\overline{\Gamma K}$ (bottom part), and a two-dimensional map (top part) for the S_1 band and its spin orientations. The arrows indicate the spin orientation for the S_1 state, and the red (blue) and white colors show the positive (negative) and zero values of the out-of-plane spin polarization, respectively.

are in agreement with a previous report for TSS [24]. The S_1 in figure 2(d) is also visible as the hexagonal-shaped CECs at $E_B = 0.75$ eV. The CEC for the inner part of S_1 evolves into a circular shape upon approaching the crossing point (E_C), and again into a hexagonal-shape in going further to deeper E_B, but the shape is rotated by 90° with respect to the CEC above the crossing point. On the other hand, the outer part of S_1 exhibits a snowflake-like pattern down to 1 eV and disappears below 1 eV. Here, we find that the characteristic deformation is abnormal for S_1 at the band top, and is rotated by 90° with respect to the TSS.

To unravel the spin characteristics of S_1, we performed the spin-ARPES measurement excited with unpolarized He I_α light ($h\nu$ = 21.223 eV). Figure 3(a) shows the spin-resolved energy distribution curves (EDCs) for E_B = 0-2.3 eV for several emission angles along the $\overline{\Gamma M}$ line. Here, spin-up and spin-down spectra are plotted with upright and inverted triangles, respectively. In the EDC for normal emission, two features are observed at E_B = 1.75 and 1.25 eV in both spin channels. The peak around 1.75 eV shifts to higher E_B as $|\theta|$ increases.

Since these features are almost spin degenerate and the band shape also changes as a function of $h\nu$, as shown in figures 1(b)–(e), this can be assigned to the bulk-derived state. For the prominent S_1 state, the spin-up peak shifts to higher E_B with increasing θ from 0 to 2.3°, and splits into two branches from 3.8°. We also notice that one spin-down branch shifts to lower E_B and another branch moves to lower E_B up to 0.7°and higher E_B above 0.7°. For negative θ, we observe the same $E - k$ dispersion but with opposite spin polarization signs. This result clearly shows that the S_1 band is spin-split and the spin orientation is antisymmetric with respect to the $\bar{\Gamma}$ point. We also find that the lower-E_B branch of S_1 is followed by weak features of the opposite spin spectra in the limited range of theta ($-5.3 < \theta < -1.3$, $2.3 < \theta < 5.3$), as indicated by the open circles. The intensities of these peaks do not exceed those for the opposite spin channel at the same E_B, even if the photon energy is changed (not shown here). Moreover, we can observe a shoulder structure for the opposite spin channel at the same E_B as the weak peak indicated by the circles at $\theta = \pm 2.3°$. This result implies that these peaks have no spin polarization. We believe that the lower-E_B branch of S_1 stems from a bulk state corresponding to the weak broad structure (B) shown in figures 1(b)–(e). In figures 3(b), we assigned spin characters to the dominant spectral features in the contour plot using upright and inverted triangles. It is identified that there is another spin-split band (S_2). This S_2 state is not clearly noticed from the ARPES results in figure 1, because it overlaps considerably with the S_1 band in a wide momentum range, and the relevant spectral weight is weak. The S_2 state also shows a spin-splitting with an antisymmetric spin orientation with respect to the $\bar{\Gamma}$ point.

As the most important experimental finding, the spin polarized band S_1 is found to show gigantic Rashba spin-splitting. Now, we try to get more insight into this particular band. Generally, the Rashba Hamiltonian without considering crystal symmetry is given by equation (1). In many cases, the Rashba parameter representing the magnitude of Rashba spin-splitting is experimentally estimated by $|\alpha_R| = 2E_R/k_0$ from the ARPES results. In the present material, E_R and k_0 are 0.5 eV and 0.135 Å^{-1}, respectively. Using these values, we can estimate $|\alpha_R| = 7.4\ \text{eV} \cdot \text{Å}$, which is more than twice as large as the reported value for the 'giant Rashba system' [14, 18, 19]. Moreover, the more important parameters E_R and k_0 show sufficient magnitudes to realize a few nanometer-sized spin current devices operated at room temperature. The Rashba spin-split band with such large E_R and k_0 has thus been discovered for the first time, and we call this the 'gigantic Rashba effect'.

Next, we perform the spin-ARPES measurement of the Rashba spin-split band along $\overline{\Gamma K}$ to explore its spin texture, as shown in figure 3(c). Here, the effective Hamiltonian of the spin-orbit interaction with a combination of three-fold symmetry is expressed by [36]

$$H_R^{C_{3v}}(\mathbf{k}) = \left(\alpha_1 + \alpha_3^1 k^2\right)\left(k_x\sigma_y - k_y\sigma_x\right) + \alpha_3^2 k^3 \cos 3\phi\sigma_z \tag{3}$$

Here, $\mathbf{k}_x$ and $\mathbf{k}_y$ correspond to the wave vectors along the $\overline{\Gamma K}$ and $\overline{\Gamma M}$ directions, and $\phi = \arccos\left(k_x/k\right)$. When the warping parameter α_3^2 is non-zero, a deformation of CECs takes place and the out-of-plane spin component emerges in the spin-split band along $\overline{\Gamma K}$ at the same time. Figure 3(c) shows that the spin-ARPES results resolve the in-plane (P_y) and out-of-plane (P_z) spin components at $\theta = \pm 5°$, corresponding to the wavenumber near the top of the S_1 band

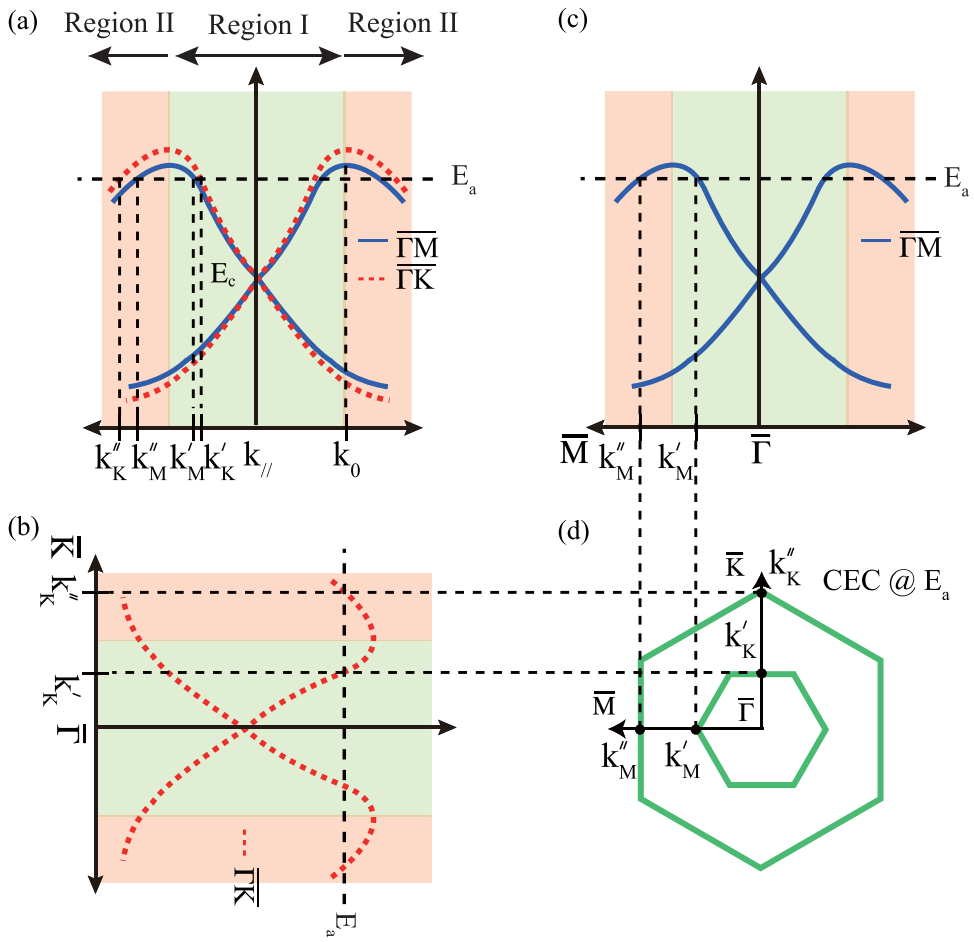

Figure 4. (a)–(c) Schematic figure for the Rashba spin-split band along $\overline{\Gamma K}$ (dashed line) and $\overline{\Gamma M}$ (solid line). (d) The anisotropic constant energy contours (CECs) at E_a.

along $\overline{\Gamma K}$. The in-plane spin-resolved EDC at $\theta = 5°$ in figure 3(c) shows the spin-up and spin-down peaks at 1.75 and 0.85 eV, respectively, both of which correspond to the spin-split S_1 band, while the spin-up peak at 2.2 eV comes from the S_2 state. It is also noted that the spin-up and spin-down peaks of the S_1 state show a distinct out-of-plane spin component. This result implies that the observed deformation of CECs is explained by a hexagonal warping effect, as represented by equation (3). Figure 3(d) schematically shows the experimentally observed spin texture. Here, the arrows exhibit spin vectors determined from our spin-ARPES result by taking the C_{3V} crystal symmetry into account. The red (blue) and white colors show the positive (negative) and zero values of the out-of-plane spin polarization, respectively. The out-of-plane spin component takes a maximum at the $\overline{\Gamma K}$ direction and the in-plane spin component shows a helical spin texture. The spin features and CECs for each surface state resemble Bi/Ag(111), which is well known to show the giant Rashba effect. A strong in-plane potential gradient related to the warping parameter α_3^2 might also be a trigger of the gigantic Rashba effect in this system, as theoretically explained for Bi/Ag(111) [14, 36, 42]. Moreover, the sign of the in-plane spin component for the S_1 state at 1.75 eV is identical to that for the S_2 state located at

2.2 eV. Nevertheless, each out-of-plane spin component becomes the opposite. The difference in the out-of-plane spin component for S_1 and S_2 implies that the sign of α_3^2 for S_1 is reversed in comparison with that of S_2. The origin of the observed sign reversal in the out-of-plane spin polarizations is unknown at present. However, if we assume that the charge densities of S_1 and S_2 residing at the topmost and bottom Te (Bi) layers in one quintuple layer on the surface or vice versa are rotated 180° to each other, then the out-of-spin polarization could change its sign. Different orbital symmetries could also explain the observed sign reversal.

Finally, we discuss the hexagonal deformation in CECs of S_1, which is rotated by 90° with respect to that for TSS. At one constant energy (E_a) above the crossing point, as shown in figure 4(a)–(c), the band dispersion along the $\overline{\Gamma M}$ line ($\overline{\Gamma K}$ line) crosses two points, k'_M and k''_M (k'_K and k''_K). In figure 4(a), the band dispersion along the $\overline{\Gamma K}$ line is steeper than that along the $\overline{\Gamma M}$ for $\mathbf{k}_{\parallel} < |\mathbf{k}_0|$ (Region I), and thus k'_M becomes longer than k'_K. On the other hand, for $\mathbf{k}_{\parallel} > |\mathbf{k}_0|$ (Region II), k''_M becomes smaller than k''_K. Consequently, the observed CECs are different in two regions. (1) In the region of $\mathbf{k}_{\parallel} < |\mathbf{k}_0|$, the CEC shows a hexagonal shape with vertices in the $\overline{\Gamma M}$ line, as is typically found for TSS. (2) For $\mathbf{k}_{\parallel} > |\mathbf{k}_0|$, the hexagonal shape or snowflake-like pattern of CEC is rotated by 90°. The resulting constant energy contours at E_a are drawn in figure 4(d). As one can see from figure 4(b)–(d), the outer CEC (Region II) shows a hexagonal shape that is rotated by 90° with respect to the inner one (Region I) and also to the TSS (see figure 2(a)). The two CECs are merged into one around the top of the band. By considering the fact that the outer CEC shows a stronger spectral weight than that of the inner one, which is probably due to the photoemission matrix element effect, we can understand that the anisotropic constant energy contour at 0.75 eV for S_1 is rotated by 90° with respect to those of TSS and S_1 at 1.55 eV, as shown in figure 2.

4. Summary

Gigantic Rashba spin-split bands have been observed in the topological insulator Bi_2Te_2Se by the ARPES and spin-ARPES experiments. The two-dimensional constant energy contours, as well as their spin textures, clearly show the peculiarity in the warping effect. Importantly, the magnitude of the Rashba parameter is found to be large enough to realize a few nanometer-sized spin current electronic devices. Moreover, two different spin-split S_1 and S_2 states possess warping parameters with the opposite sign, even in the same crystal. This novel finding opens a pathway to studies of exotic electrical and optical phenomena driven by the gigantic Rashba effect.

Acknowledgments

The ARPES and spin-ARPES experiments were performed with the approval of the Proposal Assessing Committee of HSRC (proposal nos. 12-A-28, 12-B-16 and 13-A-23). A portion of this work has been done under the Japan–Russia Bilateral Joint Research Project (JSPS). This work was financially supported by KAKENHI (grant nos. 23340105, 23244066, 25800179), Grant-in-Aid for Scientific Research (A), (B) and for Young Scientists (B) of JSPS. KAK and

OET acknowledge financial support by the RFBR (grant nos. 13-02-92105 and 12-02-00226), and by the Ministry of Education and Science of the Russian Federation.

References

[1] Bychkov Y A and Rashba E I 1984 *JETP Lett.* **39** 78
[2] Datta S and Das B 1990 *Appl. Phys. Lett.* **56** 665
[3] Nitta J, Akazaki T, Takayanagi H and Enoki T 1997 *Phys. Rev. Lett.* **78** 1335
[4] Miron I M, Gaudin G, Auffret S, Rodmacq B, Schuhl A, Pizzini S, Vogel J and Gambardella P 2010 *Nature Mater.* **9** 230–4
[5] Rotenberg E, Chung J W and Kevan S D 1999 *Phys. Rev. Lett.* **82** 4066
[6] LaShell S, McDougall B A and Jensen E 1996 *Phys. Rev. Lett.* **77** 3419
[7] Reinert F, Nicolay G, Schmidt S, Ehm D and Hüfner S 2001 *Phys. Rev.* B **63** 115415
[8] Hoesch M, Muntwiler M, Petrov V N, Hengsberger M, Patthey L, Shi M, Falub M, Greber T and Osterwalder J 2004 *Phys. Rev.* B **69** 241401(R)
[9] Hirahara T *et al* 2008 *New J. Phys.* **10** 083038
[10] Takayama A, Sato T, Souma S and Takahashi T 2011 *Phys. Rev. Lett.* **106** 166401
[11] Kadono T, Miyamoto K, Nishimura R, Kanomaru K, Qiao S, Shimada K, Namatame H, Kimura A and Taniguchi M 2008 *Appl. Phys. Lett.* **93** 252107
[12] Sugawara K, Sato T, Souma S, Takahashi T, Arai M and Sasaki T 2006 *Phys. Rev. Lett.* **96** 046411
[13] Koroteev Y M, Bihlmayer G, Gayone J E, Chulkov E V, Blügel S, Echenique P M and Hoffmann Ph 2004 *Phys. Rev. Lett.* **93** 046403
[14] Ast C R, Henk J, Ernst A, Moreschini L, Falub M C, Pacilé D, Bruno P, Kern K and Grioni M 2007 *Phys. Rev. Lett* **98** 186807
[15] Meier F, Dil J H, Lobo-Checa J, Patthey L and Osterwalder J 2008 *Phys. Rev.* B **77** 165431
[16] Yaji K, Ohtsubo Y, Hatta S, Okuyama H, Miyamoto K, Okuda T, Kimura A, Namatame H, Taniguchi M and Aruga T 2010 *Nat. Commun.* **1** 1016
[17] Shikin A M, Varykhalov A, Prudnikova G V, Usachov D, Adamchuk V K, Yamada Y, Riley J D and Rader O 2008 *Phys. Rev. Lett.* **100** 057601
[18] Park J, Jung W, Jung M-C, Yamane H, Kosugi N and Yeom H W 2013 *Phys. Rev. Lett.* **110** 036801
[19] Ishizaka K *et al* 2011 *Nat. Mater.* **10** 521
[20] Landolt G *et al* 2012 *Phys. Rev. Lett.* **109** 116403
[21] Okuda T *et al* 2010 *Phys. Rev.* B **82** 161410(R)
[22] Dil J H 2009 *J. Phys. Condens. Matter* **21** 403001
[23] Miyamoto K *et al* 2012 *Phys. Rev. Lett.* **109** 166802
[24] Arakane T, Sato T, Souma S, Kosaka K, Nakayama K, Komatsu M, Takahashi T, Ren Z, Segawa K and Ando Y 2012 *Nature Comms.* **3** 636
[25] Hasan M Z and Kane C L 2010 *Rev. Mod. Phys.* **82** 3045
[26] Frantzeskakis E and Grioni M 2011 *Phys. Rev.* B **84** 155453
[27] Souma S, Kosaka K, Sato T, Komatsu M, Takayama A, Takahashi T, Kriener M, Segawa K and Ando Y 2011 *Phys. Rev. Lett.* **106** 216803
[28] Hochstrasser M, Tobin J G, Rotenberg E and Kevan S D 2002 *Phys. Rev. Lett.* **89** 216802
[29] Xia Y, Qian D, Hsieh D, Wray L, Pal A, Lin H, Bansil A, Grauer D, Hor Y S, Cava R J and Hasan M Z 2009 *Nature Phys.* **5** 398
[30] Chen Y L *et al* 2009 *Science* **325** 178
[31] Kuroda K *et al* 2010 *Phys. Rev. Lett.* **105** 146801
[32] Hsieh D *et al* 2009 *Nature* **460** 1101

[33] Kuroda K *et al* 2010 *Phys. Rev. Lett.* **105** 076802
[34] Miyamoto K, Kimura A, Kuroda K, Okuda T, Shimada K, Namatame H, Taniguchi M and Donath M 2012 *Phys. Rev. Lett.* **108** 066808
[35] Miyamoto K, Kimura A, Okuda T, Shimada K, Iwasawa H, Hayashi H, Namatame H, Taniguchi M and Donath M 2012 *Phys. Rev.* B **86** 161411(R)
[36] Vajna Sz, Simon E, Szilva A, Palotas K, Ujfalussy B and Szunyogh L 2012 *Phys. Rev.* B **85** 075404
[37] Fu L 2009 *Phys. Rev. Lett.* **103** 266801
[38] Eremeev S V *et al* 2012 *Nature Commun.* **3** 635
[39] Henk J, Ernst A, Eremeev S V, Chulkov E V, Maznichenko I V and Mertig I 2012 *Phys. Rev. Lett.* **108** 206801
[40] Nurmamat M *et al* 2013 *Phys. Rev.* B **88** 081301
[41] Okuda T, Miyamoto K, Miyahara H, Kuroda K, Kimura A, Namatame H and Taniguchi M 2011 *Rev. Sci. Instrum.* **82** 103302
[42] Premper J, Trautmann M, Henk J and Bruno P 2007 *Phys. Rev.* B **76** 073310